Arch. Metall. Mater. **65** (2020), 1, 459-470

DOI: 10.24425/amm.2020.131748

S. PARSAMEHR[1*], A. BOOCHANI[1], E. SARTIPI[1], M. AMIRI[1],
S. SOLAYMANI[2], S. NADERI[3], A. AMINIAN[4]

MECHANIC, HALF-METALLIC AND THERMOELECTRIC PROPERTIES OF THE PdZrTiAl UNDER PRESSURE: A DFT STUDY

The half-metallic, mechanical, and transport properties of the quaternary Heusler compound of PdZrTiAl is discussed under hydrostatic pressures in the range of –11.4 GPa to 18.4 GPa in the framework of the density functional theory (DFT) and Boltzmann quasi-classical theory using the generalization gradient approximation (GGA). By applying the stress, the band gap in the minor spin increases so that the lowest band is obtained 0.25 eV at the pressure of –11.4 GPa while the maximum gap is calculated 0.9 eV at the pressure of 18.4 GPa. In all positive and negative pressures, the PdZrTiAl composition exhibits a half-metallic behavior 100% spin polarization at the Fermi level. It is also found that applying stress increases the Seebeck coefficient in both spin directions. In the minority spin, the *n*-type PdZrTiAl, the power factor (PF) for all the cases is greater in the equilibrium state than the strain and stress conditions whereas in the majority spin, the PF value of the stress state is greater than the other two. The non-dimensional figure of merit (*ZT*) is significant and is about one in spin down in the room temperature for the all pressure states that it remains on this value by applying pressure. The obtained elastic constants indicate that the PdZrTiAl crystalline structure has a mechanical stability. Based on the Yong (E), Bulk (B) and shear (G) modulus and Poisson (n) ratio, the brittle-ductile behavior of this compound has been investigated under pressure. The results indicate that PdZrTiAl has a ductile nature and it is a stiffness compound in which elastic and mechanical instability increases by applying strain.

Keywords: PdZrTiAl, Half-metal, Thermoelectric, Elastic constants, DFT

1. Introduction

Lastly, the Heusler compounds were taken into consideration due to their various properties including the half-metals [1,2], spin-gapless half-metals, spin-gapless semiconductors [3,4] and topology insulators [5,6]. These compounds have several crystal structures such as full-Heusler (X_2YZ) [7,8], half-Heusler (XYZ) [9,10], DO3 [11,12] and tetragonal [13,14] which all of these structures have the same crystallography structures. In the full-Heuslers, the X and Y atoms belong to the transition metals and Z is one in the III-V column of the periodic table. If one of the X atoms is replaced with another atoms (M), the new Heusler compounds are formed named the equiatomic quaternary Heuslers with $F\bar{4}3m$ (216) space group [15,16].

The study of half-metallic Heusler compounds has gained significant momentum over the last decade due to their exceptional qualities in displaying wide varieties of properties, ranging from half-metallic magnetism, magnetic shape memory effect, spin gapless semiconductor to giant magnetocaloric effect, thermoelectric effect and superconductivity [17-22]. These properties have been exploited successfully for technological applications. For example, the half-metallicity in ferromagnetic materials is being used for spintronic applications such as spin injectors [23], magnetic tunnel junctions [24], spin valves [25] and spin torque transfer-random access memories [26]; the zero gap traits in spin gapless semiconductors is being used for studying spin Seebeck effect [27]. The largest numbers of magnetic Heusler compounds investigated are ternary half-metallic X2YZ where X and Y are transition metals and Z is a main group element. It is obvious that the novel magnetic properties in these compounds arise due to the presence of unfilled *d* orbital of more than one transition metal components. An intricate relationship between the occupancies of the magnetic constituents in sub-lattices with different symmetries,

[1] DEPARTMENT OF PHYSICS, KERMANSHAH BRANCH, ISLAMIC AZAD UNIVERSITY, KERMANSHAH, IRAN.
[2] HARSIN BRANCH, ISLAMIC AZAD UNIVERSITY, HARSIN, IRAN.
[3] YOUNG RESEARCHERS AND ELITE CLUB, KERMANSHAH BRANCH, ISLAMIC AZAD UNIVERSITY, KERMANSHAH, IRAN.
[4] DEPARTMENT OF PHYSICS, UNIVERSITY OF GUILAN, RASHT, IRAN.

* Corresponding author: sajadparsamehr@gmail.com

the magnetic structures associated and the electronic structures resulting due to these two have been found to be responsible behind the emergence of the novel phenomena observed in these materials. If each sub-lattice, in a Heusler structure, is occupied by a different element, resulting in a XX′YZ compound, with X′ a magnetic element different than X, then there will be more sub-classes (depending on the sub-lattice occupancies of the three magnetic elements) of the structure than that possible with X2YZ compounds.

Several investigations [28-38] on the HMMs have been done based on equiatomic quaternary Heusler structure (EQH) (LiMgPdSn – structure, space group *F*-43*m* (216)). Compared with the pseudo ternary Heusler HMMs, the EQH ones have the advantage of lower power dissipation due to the less amount of disorder that exists in them [39].

So far, Heusler compounds based on Zr atom have been studied exhibiting half-metallic or semiconductor behaviors with zero gap [40-42]. Among these, quaternary combinations like ZrVTi(Al,Ga) and ZrMnVZ (Z = Si,Ge) are predicted which are ferromagnetic half-metals [43,44], or compounds such as ZrCoCrBe and ZrCoVIn can have spin-gapless semiconductor features [45,46]. Recently, the physical properties of the new structure of the quaternary Heusler compound, PdZrTiAl, have been studied based on the first principle calculations. The results show the half-metallic ferromagnetic behavior of this Heusler alloy, the presence of indirect gaps in the minority spin with a value of about 0.66eV and the spin flip gap of about 0.49eV. The magnetic moment obtained from the Slater-Pauling rule is the integer amount of $3\mu_B$ [47]. Half-metallic ferromagnets are supposed to exhibit a real gap in the minority density of states where the Fermi energy is pinned. The gap has the consequence that the number of occupied minority states has to be an integer. Thus, the Slater-Pauling rule will be strictly fulfilled with $M_{tot} = (N_v - 18)$ for the spin magnetic moment per atom for the half-Heusler cases by $F\bar{4}3m$ space group.

Therefore, due to the small gap of PdZrTiAl in the minority spin which is required for good thermoelectricity in the material and this fact that the thermoelectricity of this material has not been studied so far, this compound is appealing to study. It is noteworthy that by applying the hydrostatic pressure, the atoms in the unit cell become closer or farther, so the material behavior is expected to change under stress and strain. Hence, the variation range of the half-metallic behavior of this compound was studied by applying a limited hydrostatic pressure, and it was observed that the spin gap has changed under the pressure as well as the thermoelectric quality, especially in the spin down at high temperatures.

Thermoelectric (TE) power generation is currently taking increasing interest as it uses waste heat for useful purposes, and materials with high values of Seebeck coefficient are required to achieve this goal. The high Seebeck coefficient values are commonly obtained in materials with narrow band gap semiconductors, low values of carrier concentration [48]. Like thermoelectric power generation, the thermoelectric cooling is also important. Thermoelectric cooling requires low-temperature materials, however, the literature lacks the study of low-temperature as compared to Thermoelectric (TE) materials of high temperature, and the studies of the metallic TE materials are scanty [49,50].

The principal goal for all these studies was to develop materials with the highest maximal ZT efficiency. Recently, researchers started working on quaternary or ternary based chalcogenides like CuGaTe2 [51], Cu2CdSnSe4 [52-53], CuInTe2 [54-57], Cu3SbX4 (X = Se, S) [58,59] and Cu2ZnSnX4 (X = Se, S) [60,61], which may be considered as modified forms of II-VI ZnS semiconductors. Due to their comparatively low value of thermal conductivity and exceptional properties of electrical transport, these materials may be used as potential thermoelectric [62-67]. In this work, since pressure, as a sensitive characteristic, plays an important role in the structural and electronic properties of materials, the physical properties of the PdZrTiAl Heusler composition, including structural, electronic, mechanical, and thermoelectric properties, has been studied in the temperature range from 50 to 800K under hydrostatic pressure using the density functional theory and Boltzmann quasi-classical theory.

2. Computational Details

The initial structure of PdZrTiAl was optimized in the framework of the density functional theory [68] based on the full-potential linearized augmented plane wave (FP-LAPW) method using the WIEN2k code [69]. The Perdew-Burke-Ernzerhof version of the generalized gradient approximation for solids (GGA-PBEsol) [70] was used to calculate the structural, elastic and electronic properties. The Muffin-tin radius was chosen in a way to have no charge leakage. In order to achieve the best convergence, limits such as the basis set is expanded in terms of the plan wave up to RmtKmax=7, and Kpoint=3000 is applied for the integration of the Brillouin zone with 14×14×14 mesh in the Monkhorst-Pack grids [71,72]. The total energy convergence is set on 1×10^{-5}eV/atom, the self-compatible field on 1×10^{-7}eV/atom, the maximum ion force on 0.1 eV/Å and the maximum value of stress ≤0.02 GPa. The hydrostatic pressures range (–11.4, –8.1, 8.8, and 18.3 GPa) obtained from the Murnaghan diagram was applied according to the third-order Birch-Murnaghan equation (EOS) [73].

$$P = \frac{3}{2}B_0\left[\left(\frac{V}{V_0}\right)^{-7/3} - \left(\frac{V}{V_0}\right)^{-5/3}\right]\times \left\{1 + 3/4\left(B_0' - 4\right)\left[\left(\frac{V}{V_0}\right)^{-2/3} - 1\right]\right\} \quad (1)$$

In addition, the thermoelectric properties of this Heusler compound, such as electrical conductivity and Seebek coefficient, are obtained using the BoltzTraP quasi-classical code [74,75].

3. Result and Discussion

3.1. Structural Properties

The quaternary crystal structure of PdZrTiAl is theoretically predicted by Saadi Berri in the form of a LiMgPdSn-type structure with spatial symmetry of $F\bar{4}3m$ [47]. In its primary cell, the atoms of Pd, Zr, Ti and Al are positioned in the Wyckoff positions, 4d(3/4,3/4,3/4), 4b(1/2,1/2,1/2), 4c(1/4,1/4,1/4) and 4a(0,0,0), respectively. The values of the lattice constants, the Bulk modulus, the optimized volume curves and the hydrostatic pressures that are listed in Table 1 are obtained by the self-consistent solution of the total energy and Birch-Murnaghan equation [73] at zero pressure which they have a good agreement with the predicted theoretical values. According to the E-V curve and also the resulting formation energy values, it is well-known that the PdZrTiAl composition is structurally more stable in terms of being under the highest positive pressure of 18.3GPa (Fig. 1).

TABLE1

The Density ρ(gr/cm^3), lattice parameter a(Å) and formation energy E_f(Ryd) of the PdZrTiAl compound under pressure

	ρ (gr/cm^3)	a(Å)	E_f(Ryd)
PdZrTiAl	6.5631	6.554	–0.332179
P_1(18.3 GPa)	7.2999	6.2822	–0.324736
P_2(8.28 GPa)	6.9155	6.3936	–0.329998
P_3(–8.1 GPa)	5.9726	6.7169	–0.329232
P_4(–11.4 GPa)	5.7128	6.8172	–0.325398

3.2. Electronic Properties

The electron density of states (DOS) diagram gives very important information about the electron structure of matter in which determines the probability of an electron at each energy level.

Moreover, knowing the band gap is important for determining the thermoelectric function of the material. Thus, the precise value of the thermo power parameter (Seebeck coefficient) can be calculated directly from the band gap using the Mott's relation based on the Boltzmann theory [76].

$$S = \frac{\pi^2}{3}\frac{K^2 T}{e}\frac{dLn\sigma(E)}{dE}\bigg|_{E=E_f} \tag{2}$$

which $\sigma(E)$ is the electron conductivity value as a function of Fermi energy.

In Fig. 2, the electron density of states diagram is shown for the PdZrTiAl composition under stress, strain and relaxation in a way that the applied stresses have changed from the negative to the positive. It is noteworthy that although there is no significant change in the electron density of states under the applied pressures at the Fermi range for the majority spin, significant variations can be observed at the Fermi range for the minority spin so that a tangible increase can be seen in the edge of the band gap by applying positive pressure (stress). The lowest band gap of 0.25 eV and the most band gap of 0.9 eV is calculated at the pressures of –11.4 GPa (strain) and 18.3 GPa (stress), respectively, so it can be concluded that the pressure effects on this quaternary composition lead to change in its half-

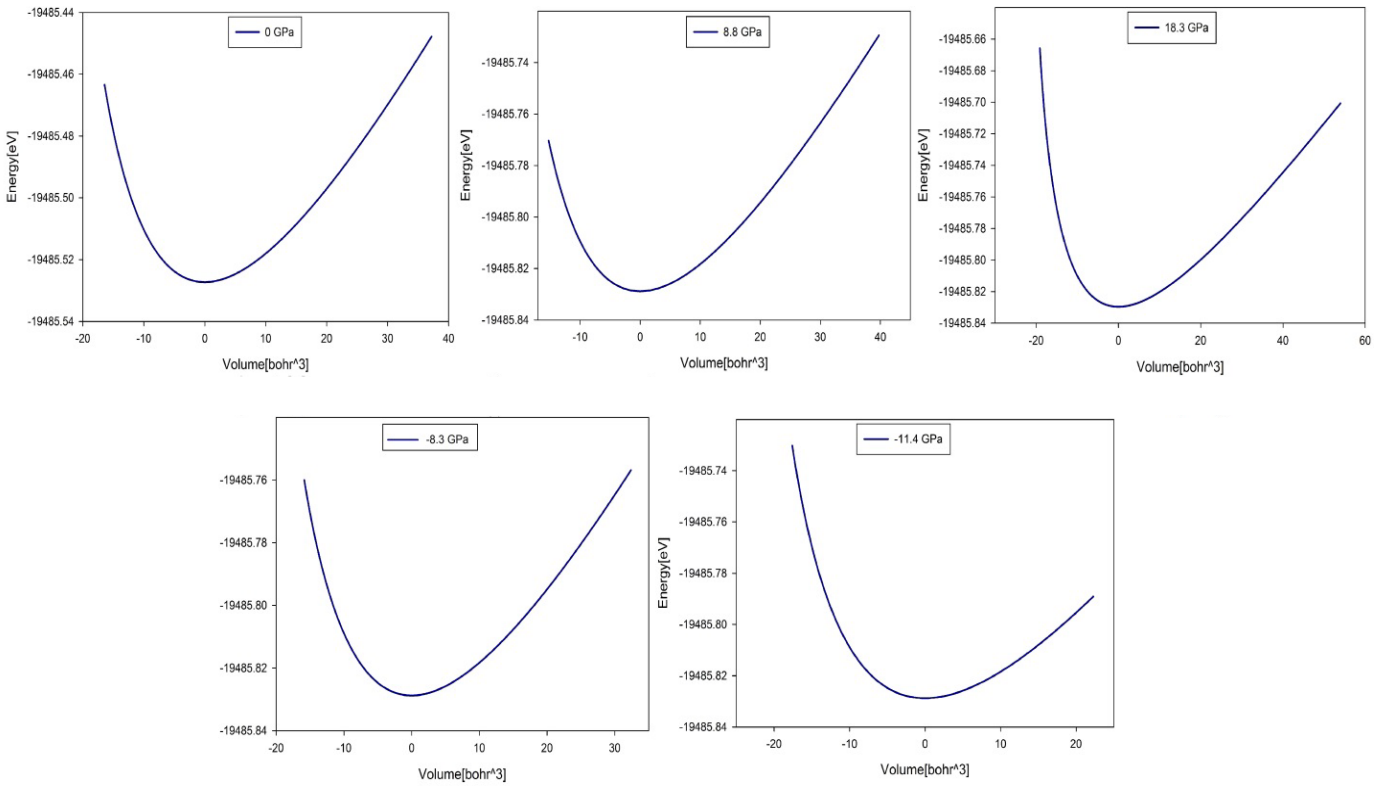

Fig. 1. The energy-volume diagrams of the PdZrTiAl on the pressures

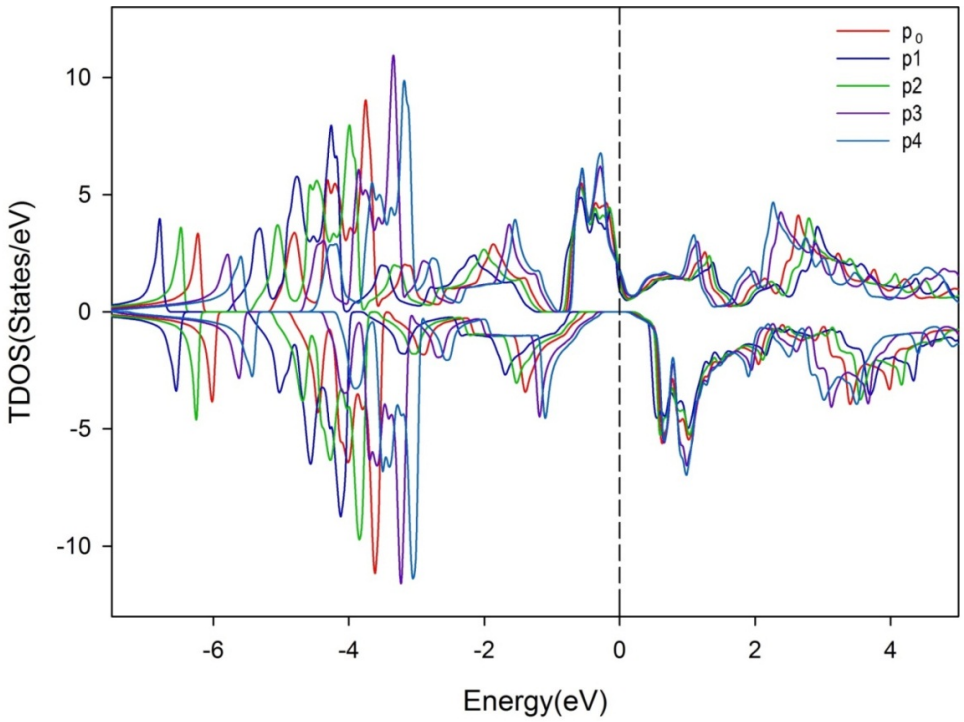

Fig. 2. The DOS diagram of the PdZrTiAl in the equilibrium pressure (P_0 = 0 GPa) and (P_1 = 18.3 GPa)

metallic behavior. Most importantly, this compound remains as a half-metal with the spin polarization of 100% at all positive and negative pressures, and it is not essentially subjected to electronic instability under pressure. Under positive pressure, the greatest influences of pressure have occurred in the valence region and the range from –8 to –1 eV for both spin directions so that the electron states shift toward lower energies, and also the peaks of the density of states in the conduction region shift toward higher energies. Generally, it can be concluded that by applying a positive pressure (stress), the electron densities of states upper and lower than the Fermi level getting away from each other. As seen from the DOS diagram, in the spin up, the continuity of the electron states at the Fermi surface, below and above it can be observed, so is the electron conductivity well at the all mentioned pressures. Moreover, the DOS curve broadening at the Fermi range in the spin up and even down represents the electrical and magnetic stabilities of this compound at the all pressures. To confirm the previous conversations in the density of the states diagram, the band structure diagrams for the PdZrTiAl composition are plotted in Fig. 3 from the pressure of –11.4 GPa to 18.3 GPa and the equilibrium pressure for two spin modes of up and down along the symmetric directions in the first Brillouin zone. As expected, in spin-up equilibrium pressure, energy levels cut off the Fermi level in several symmetric directions indicating the desire to show metallic properties in this spin. In other words, due to frequent discontinuities, the curve slope is changing, as a result, the group velocity increases and the effective mass decreases. At the opposite point, in the spin down, an indirect band gap can be seen along Γ to X with a value of 0.6 eV. Therefore, in equilibrium pressure, this quaternary compound is a half-metal with a spin polarization of 100% demonstrating a high metallic behavior in the spin up and a *n*-type semiconductor behavior in the spin down. Hence, the accumulation of electron levels in the Fermi range in spin up and an *n*-type band gap in the spin down make this compound suitable for thermoelectric purposes.

In the following, the band structure diagrams are plotted under the positive and negative pressures for comparison. As expected, at all pressures, the half-metallic behavior of this composition is maintained, but there is a band gap increase up to 0.77 eV at positive and larger pressures (18.3 GPa) so that by increasing the pressure, a perceptible change is occurred in the maximum valance bands and these levels have shifted to lower energies. On the other hand, at negative pressures, the electron levels become closer to the Fermi level, and consequently, the band gap decreases. Besides, an increase in the effective mass can be seen in this spin mode, so it can be said that a better thermoelectric effect is expected at negative pressures.

3.3. Elastic Properties

One of the physical tools analyzing the mechanical stability of materials is the elastic coefficients and their derived parameters. The PdZrTiAl composition is a cubic structure with the F.C.C base, so only three components of C_{11}, C_{12} and C_{44} are non-zero components of the elastic constants tensor. The elastic constants are listed in Table 2 for strain, stress and equilibrium pressure states as well as their dependent parameters such as the bulk modulus (B), Young modulus (E), shear modulus (G), Poisson ratio, B/G ratio, transverse and longitudinal average sound velocities, Debye temperature, and melting point. According to

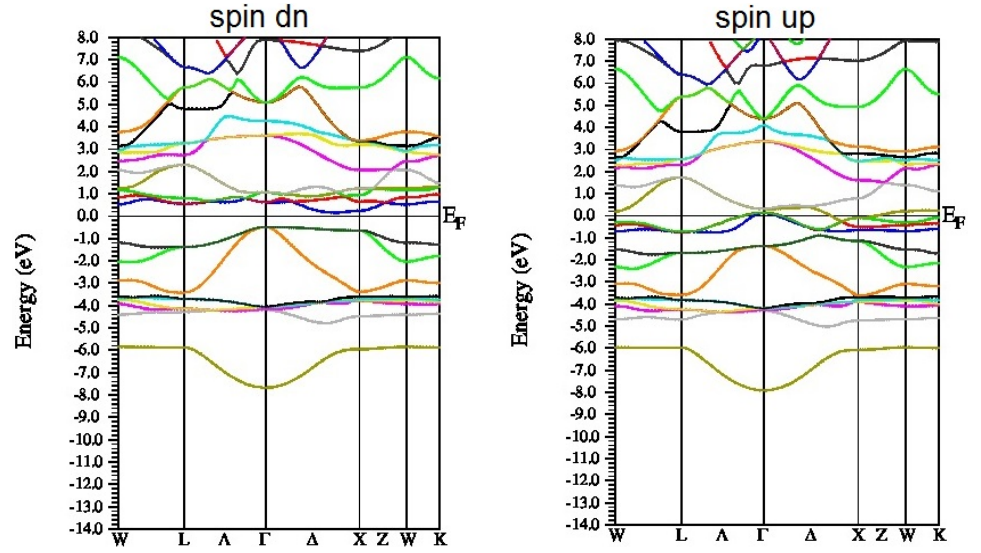

(a) P_0 = 0 (Gpa)

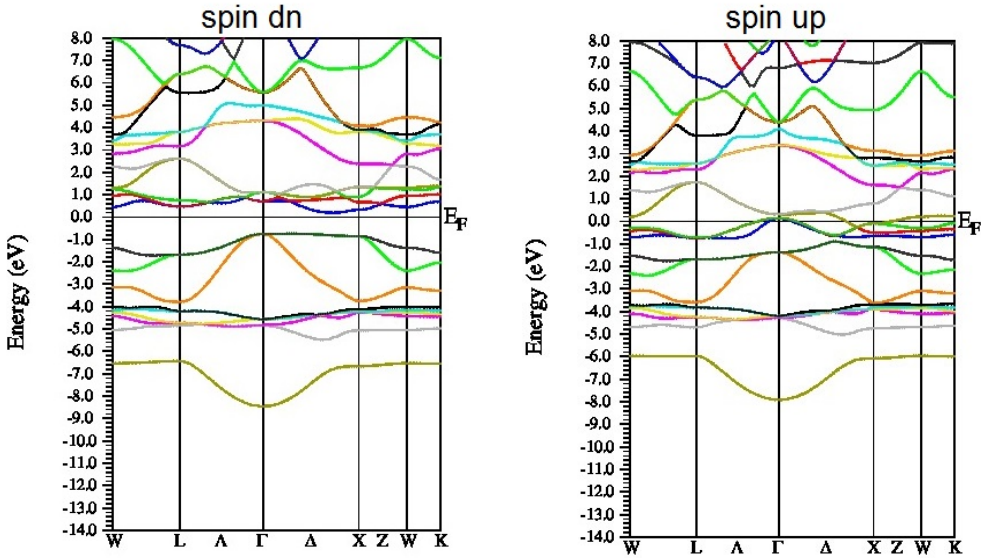

(b) P_1 = 18.3 (GPa)

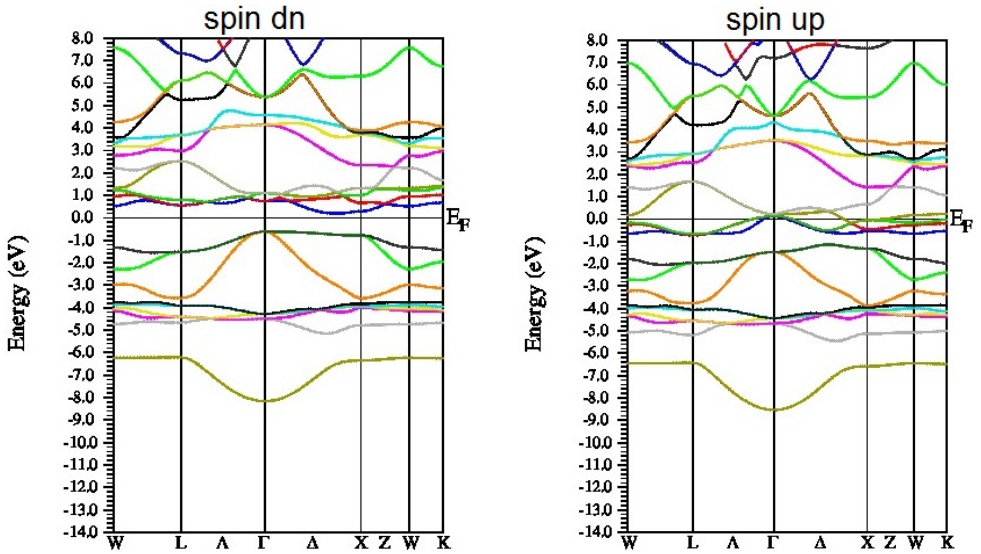

(c) P_2 = 8.8 (GPa)

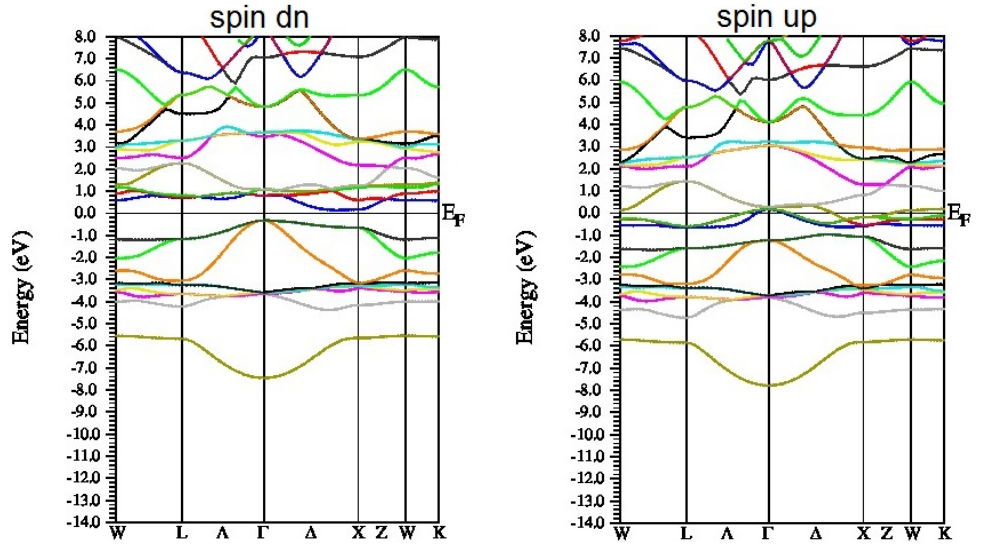

(d) P_3 = 8.1 (GPa)

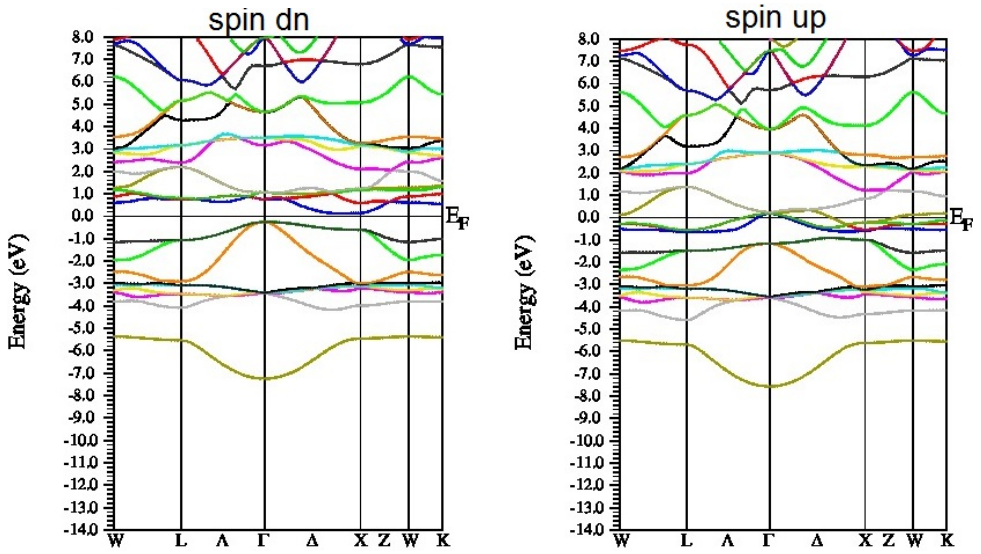

(e) P_4 = –11.4 (GPa)

Fig. 3. The band structure diagrams of the PdZrTiAl on the explained pressures

the following relationships [77], the Voigt-Reuss-Hill approximation (VRH) is used to calculate Yang and shear modules:

$$E = \frac{9BG_X}{3B + G_X} \tag{3}$$

$$C_{Voigt} = \left(C_{11} - C_{12} + C_{44}\right)/5 \tag{4}$$

$$G_{\mathrm{Re}uss} = 5\left(4S_{11} - 4S_{12} + 4S_{44}\right)^{-1} \tag{5}$$

$$G_{Hill} = \tfrac{1}{2}\left(G_{Voigt} + G_{\mathrm{Re}uss}\right) \tag{6}$$

which $S = C$-1, and X represent Reuss (R), Voigt (V), and Hill (H) as index in these relationships. The values of the bulk modulus and the Poisson ratio are obtained from the following relationships [78]:

$$v = \frac{3B - E}{6B} \tag{7}$$

$$B = \frac{C_{11} + 2C_{12}}{3} \tag{8}$$

It can be perceived that the composition is elastically stable in the equilibrium state because

$$C_{11} - C_{12} > 0, \quad C_{44} > 0$$

The numerical value of the elastic constants expresses the proper strength of this alloy in the mechanical materials and applications. Young modulus (E) represents the stiffness of materials expressing the relationship between stress and strain [79], and also the shear modulus (G) states the hardness of materials. According to Table 2, the lowest values of Yong and

shear modules are related to the strain state which by elevating E, the composition hardness rises and the nature of the covalent bond rises. Among the compared cases, bulk, shear and Yang modules have the highest values at the pressure of 18.3 GPa, so it can be said that similar to the ScTM (TM = Cu, Ag, Au and Pd) compositions], the PdZrTiAl composition has the highest stiffness and hardness at this pressure [80].

The B/G ratio indicates the mechanical strength of the material, which was identified by Pugh [78]; If this ratio is less than 1.75, the nature of the substance is brittle otherwise ductile. Additionally, if the Poisson coefficient (υ) is greater than 0.33, the nature of substance is brittle, and less than this amount, it is ductile. Thus, Poisson coefficient confirms the B/G ratio in Table 2 that the PdZrTiAl composition of has a ductile nature. As a further matter, Poisson ratio is an important quantity in measuring the material incompressibility ranging from 0 to 0.5, i.e., the incommensurability of the substance increases from 0 to 0.5. It is clear from the obtained values for u in Table 2 that the PdZrTiAl composition demonstrates a slight compressibility against deformation except for the pressure of –8.1 GPa [81,82]. Calculating the Vickers hardness number [83] from the relation $H_V = 0.92(G/B)^{1.137}G^{0.708}$ represents the highest hardness for the PdZrTiAl composition at 18.3 GPa pressure among the compared cases in Table 2.

The difference between the elastic responses for the various crystal directions (C_{11}, C_{12} and C_{44}) makes this composition an elastically anisotropic material such that its anisotropy coefficient (A) is far from 1. Therewith, the crystal hardness shows that this composition has an extremely high melting point temperature, and consequently, the average sound speed is a considerable number and the Debye temperature of this compound is about room temperature (Table 2). Accordingly, the pressure effects have caused the hardness of this compound to increase significantly. However, the elastic constants have increased as well as bulk modulus, the Poisson and the B/G ratios have decreased. In this regard, an escalation can be seen in the Yong and shear modules while the elastic anisotropy is reduced, but by applying the strain, the elastic constants is noticeably declined leading to elastic instability. Similarly, the modules of bulk, Yang and shear have reached very small values, so elastic and mechanical instabilities can be seen in strain state.

TABLE 2

The elastic constants C_{ij} (GPa), Bulk module B (GPa), Yong module E (GPa), Shear module G (GPa), the B/G ratio, Poisson coefficients υ, Anisotropy parameter A, Vickers hardness (H_v) (GPa), Debye temperature (K), Melting point (T_m (K)), Longitudinal velocity (V_l (m/s)), Transverse velocity (V_t (m/s)) and Mean velocity (V_m (m/s)) of the PdZrTiAl, under pressure

	PdZrTiAl	P_1	P_2	P_3	P_4
C_{11}	207.5	355.6	208.3	59.6	65.5
C_{12}	103.9	140.1	80.9	78.6	52.8
C_{44}	56.9	187.7	100.1	32.3	12.9
B	138.4	211.9	123.4	70.3	57
B/G	2.52	1.41	1.47	–9.12	5.87
υ	0.32	0.2	0.22	0.7	0.4
G_V	54.8	155.7	85.6	16.2	10.2
G_R	54.7	144.7	81.5	–31.7	9.1
G_H	54.8	150.2	83.5	–7.7	9.7
E_v	145.4	375.3	208.5	45.2	29.1
E_R	145.1	353.7	200.4	–112.2	26
E_H	145.3	364.6	204.5	–24.2	27.5
H_v	5.46	21.62	13.53	0.034	0.61
A	5.46	3.04	3.35	1.25	6.06
θ_D	371.8	447.2	400.6	306.4	300
T_m ±300	1537	2024	1741	1244	1135
v_l	5492.4	6762.4	5814.9	4783	4525.4
v_t	2884.8	3359.2	3054.7	2449.4	2442.4
V_m	3226.2	3744.9	3416.1	2743.7	2726.2

3.4. Thermoelectric Properties

Nowadays, the thermoelectric behaviors of Heusler compounds have been highly regarded by industry and science, since there is potential for generating electricity by applying a temperature gradient, or it is possible to transfer heat from a point to another by applying a potential electrical difference. The parameters affecting the thermoelectric phenomenon include the Seebeck coefficient (S), the electron conduction coefficient (σ), the figure of merit (ZT) and the power factor (PF). Fig. 4(a) shows the Seebeck coefficient variation for PdZrTiAl composition in two spins of up and down under pressure in the temperature range of 50 to 1000K. The Seebeck coefficient equation is in the form of the following:

$$S = \frac{8\pi^2 k_B^2}{3eh^2} m^* T \left(\frac{\pi}{3n}\right)^{2/3} \tag{9}$$

which m^*, K_B, h, n and e are in turn the values of the effective masses of the charge carrier, the Boltzmann constant, the Planck constant, the carriers concentration and the electron charge. It is observed that the Seebeck coefficient is directly proportional to temperature and indirectly to the carrier concentration (either electron or hole), so the S value follows the above relation for both spin modes. According to figure, in equilibrium, the Seebeck coefficient has a positive sign in the spin up, but a negative sign in the spin down. Hence, the behavior variation in this coefficient by changing the external field direction can be an important phenomenon for this composition, as it becomes an n-type thermoelectric in the spin down and a metal in the spin up. In the equilibrium state and the majority spin, the Seebeck coefficient begins to increase with a gentle slope by applying temperature, but this behavior is completely different in the minority spin, where there is the electrons concentration. In the spin down, the Seebeck coefficient exhibits the highest semiconductor behavior at the temperature of 50K, and it tends to smaller values with a steep slope up to 200K. After that, it experiences a mild reduction to reach –53 at 800K. By applying a positive pressure in the spin up, a significant increase can be observed for this coefficient, especially after 200K. In the strain state, the

Seebeck coefficient value in the spin up is lower than the value in the equilibrium state to the extent that it tends to really small values, which can be due to the greater effective mass created by the stress. In spin down, the highest value of this coefficient for the range of 150 to 450K is the equilibrium value which it can be seen that by applying positive pressure, the absolute magnitude of this coefficient is greater than the equilibrium value over the entire temperature range, except for the temperature of 50K, and the Seebeck coefficient in negative pressure is often close to the equilibrium value. On that account, it can be said that applying stress in both spin modes increases the Seebeck coefficient, similar to the work carried out by Donglin Guo et al. [84]. It is noteworthy that the Seebeck coefficient depends on the derivative of the density of states, that is, the slope of the DOS curve. In this regard, it can be seen from Fig. 2 which in the minority spin, the DOS curve slope in the conduction band is greater than that of the valance band resulting in an increase in the Seebeck coefficient for this *n*-type semiconductor.

In Fig. 4(b), the electron conductivity is shown in two spins of majority and minority. As expected, based on the metallic behavior of this compound in the spin up, the electron conductivity is initiated at very low temperatures and increased linearly compared to the equilibrium state, but applying the hydrostatic pressure lessen the electron conductivity so that the electron conductivity in the negative pressure is greater than that of the equilibrium and the positive pressure. In the spin down, the electron conductivity value in the equilibrium state is higher than those of the stress and strain states, which is similar to the result obtained by applying compression strain on Cu3SbSe4 composition by Muhammad Irfan et al [85]. The value of σ in this spin is zero up to the room temperature, and then it begins to increase with a sharp slope in the equilibrium state. In addition, applying pressure reduces the conductivity in this spin compared to the equilibrium state, and it is observed that this decrease is more in the stress state and it is partial in the strain one. Since the electron conductivity is related to the charge carrier mobility, it can be concluded that the pressure has affected the carrier mobility.

The electron contribution of the thermal conductivity in two spins of up and down in Fig. 4(c) expresses that the variations of this parameter with the temperature are almost linear in the spin up, but a completely different behavior is observed in spin down. At all pressures, its value is zero up to the room temperature, and then, the electrons suddenly start to run which is owing to the *n*-type semiconductor behavior of this composition in this spin. For that reason, it can be concluded that the electron conduction for this compound in the spin down starts at the room temperature. On the contrary, it can be understood that the pressure has a slight effect on the electron thermal conductivity, and for this reason, introducing pressure causes small decline in the electron thermal conductivity. The figure of merit diagram, as the most important thermoelectric quantity is dependent on the external magnetic field. In spin up, the *ZT* values are extremely minor and insignificant which it has reached about 0.13 at the ideal conditions, the pressure of 18.3GPa and the room temperature, and it has an infinitesimal amount at the equilibrium and negative pressures. In spin down, it is a significant and large value (about 0.97) under the room temperature range in all pressure states, similar to the work done on the SnSe zigzag graphene [86], so it can be considered as a thermoelectric material at low temperature, e.g. thermoelectric coolers such as the Bi2Te3 *n*-type semiconductor compound [87]. Above the room temperature, a drastic fall can be spotted for figure of merit by applying strain while applying positive pressure keeps it around the range of 1 and its values are higher than the equilibrium ones illustrating a promising structure for thermoelectric applications.

The PF quantity is investigated in Fig. 4(e). In the spin up, the power factor for the stress state is greater than those for the strain and equilibrium states, but according to Fig. 4(b), the electric conductivity of the strain is greater than equilibrium and stress states. The most important reason can be the increase in the Seebeck coefficient under stress, which greatly neutralizes the reduction in the electrical conductivity. In the spin down, the PF shows a completely different behavior so that it has a greater value in the equilibrium state than the other states. In all states of the stress, strain and equilibrium, the PF value starts from zero and it gradually elevates by increasing the temperature, so that it peaks for all three states at the temperature of 820K. It should be noted that the variation trend of the PF relative to the temperature is incremental in both spin modes.

In Fig. 4(f), the lattice contribution of the thermal conductivity is calculated. Since the BoltzTraP software does not calculate this parameter, it is therefore possible to extract the K_{latt} value using the elastic information according to the relationships provided by Slack [88].

$$K_L = A\frac{M_a V n^{1/2}\theta_D^3}{\gamma^2 T} \tag{10}$$

In this equation, M_a, n, γ, θ_D and V are the mean atomic masses, the number of atoms in the unit cell, the Grüneisen parameter, the acoustic Debye temperature, and the volume per atom, respectively. It can be observed that in both spin directions and at low temperatures, K_{latt} is a large number decreasing by increasing temperature up to 100K, and then it reaches the saturation limit with a mild slope at high temperatures.

4. Conclusion

Using the first principle study based on the density functional theory and utilizing GGA, structural, elastic, mechanical, electronic and thermoelectric properties of the PdZrTiAl quaternary composition have been investigated under hydrostatic pressures. The obtained lattice constant and bulk modulus are in a good agreement the other values. It is found that the band gap value in the minority spin increases by employing stress and decreases with strain. This means that its half-metallic behavior changes, but it eventually maintains the half-metallic properties with 100% spin polarization. The PdZrTiAl has a stable

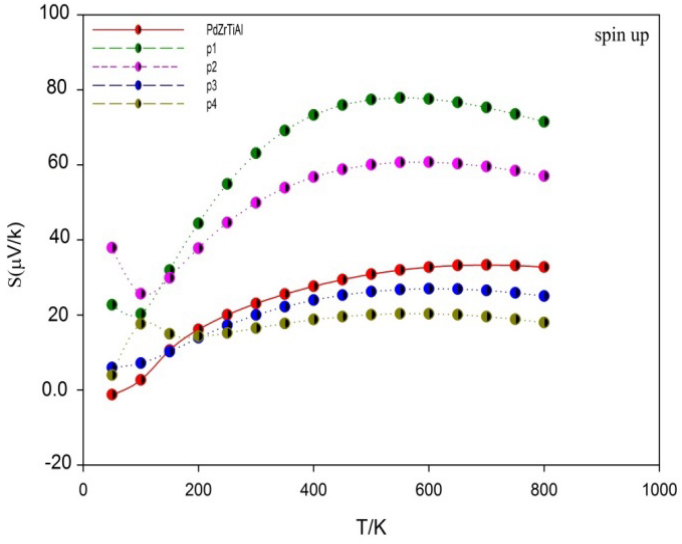
spin up
PdZrTiAl
p1
p2
p3
p4
S(μV/k)
T/K

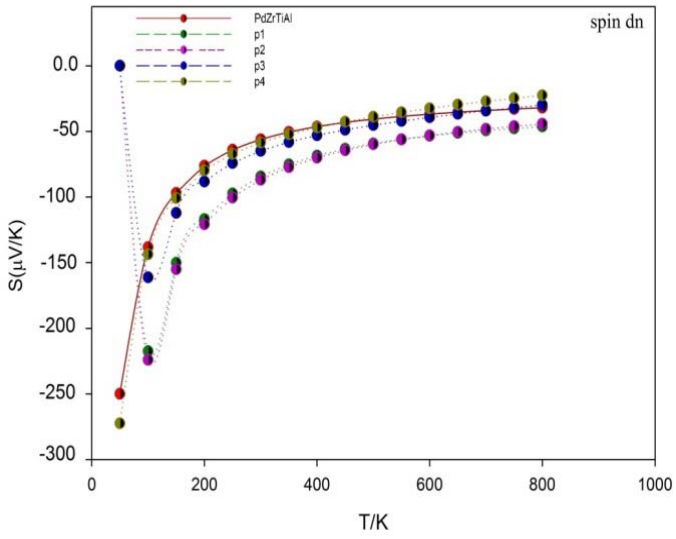
spin dn
PdZrTiAl
p1
p2
p3
p4
S(μV/K)
T/K

(a)

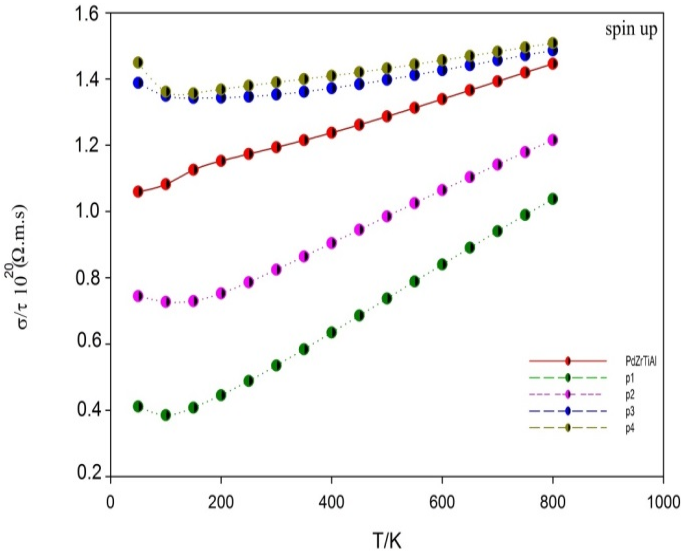
spin up
PdZrTiAl
p1
p2
p3
p4
σ/τ 10^20(Ω.m.s)
T/K

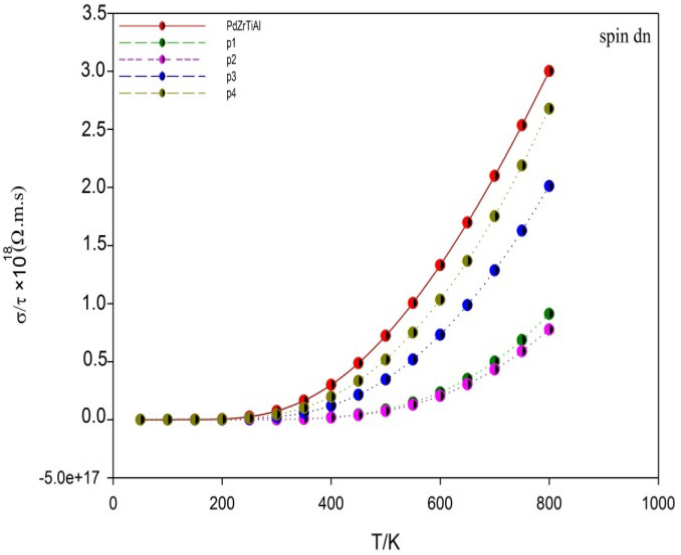
spin dn
PdZrTiAl
p1
p2
p3
p4
σ/τ ×10^18(Ω.m.s)
T/K

(b)

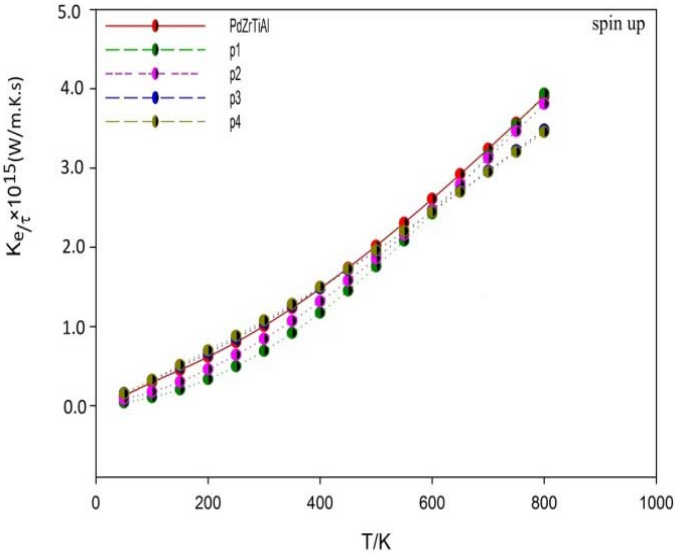
spin up
PdZrTiAl
p1
p2
p3
p4
Ke/τ×10^15(W/m.K.s)
T/K

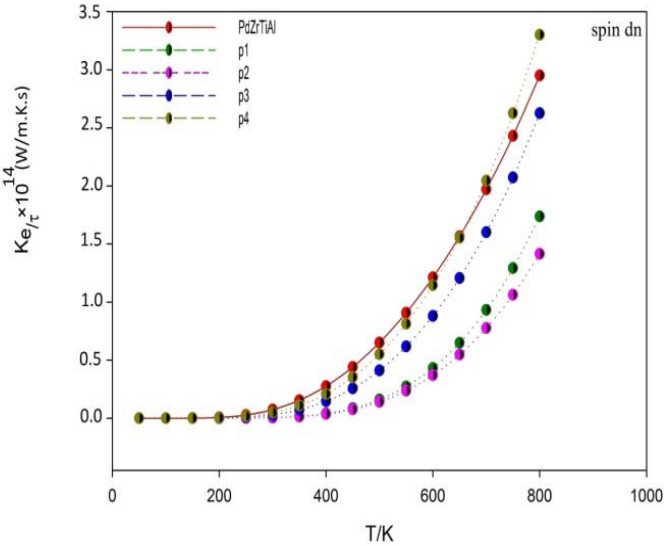
spin dn
PdZrTiAl
p1
p2
p3
p4
Ke/τ×10^14(W/m.K.s)
T/K

(c)

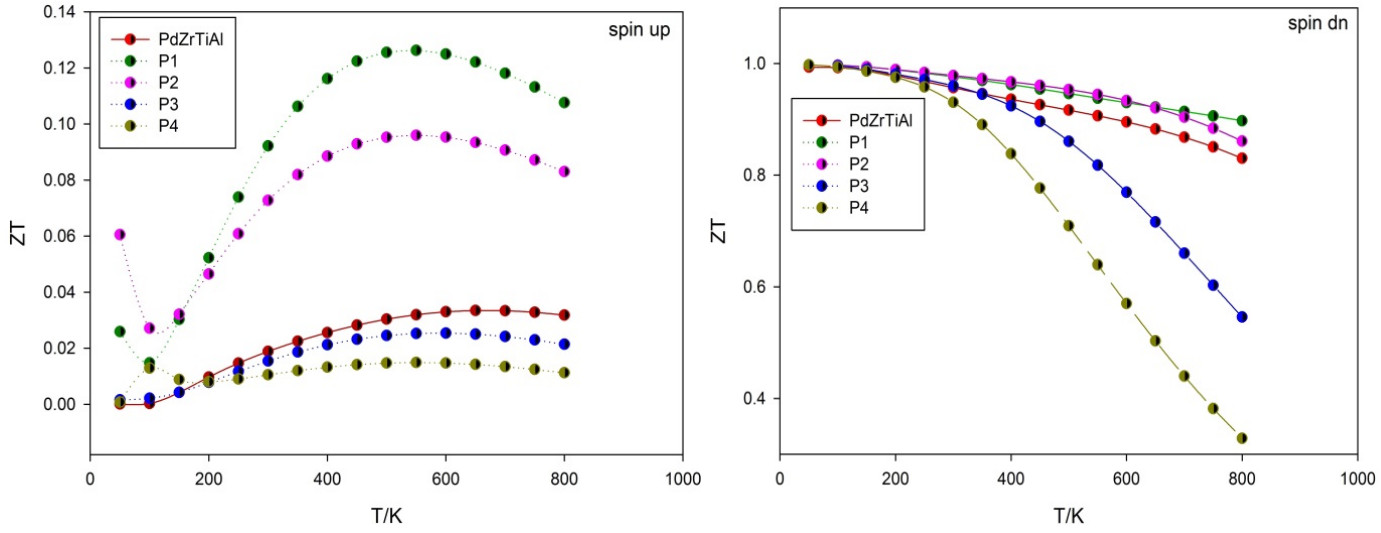

(d)

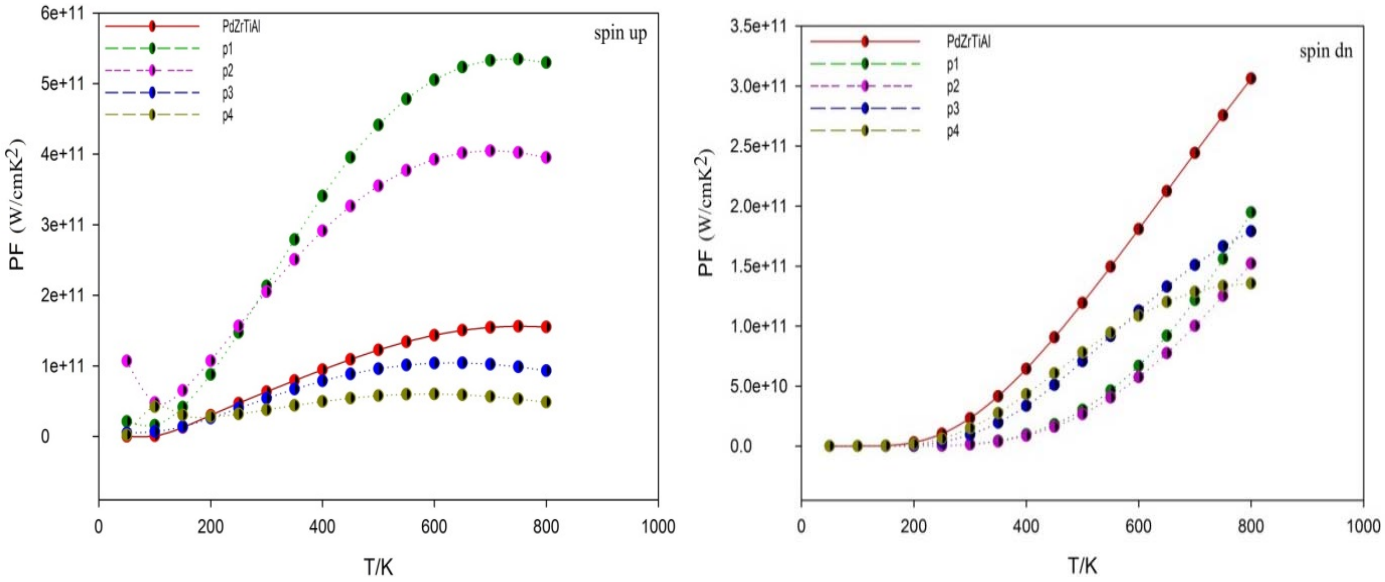

(e)

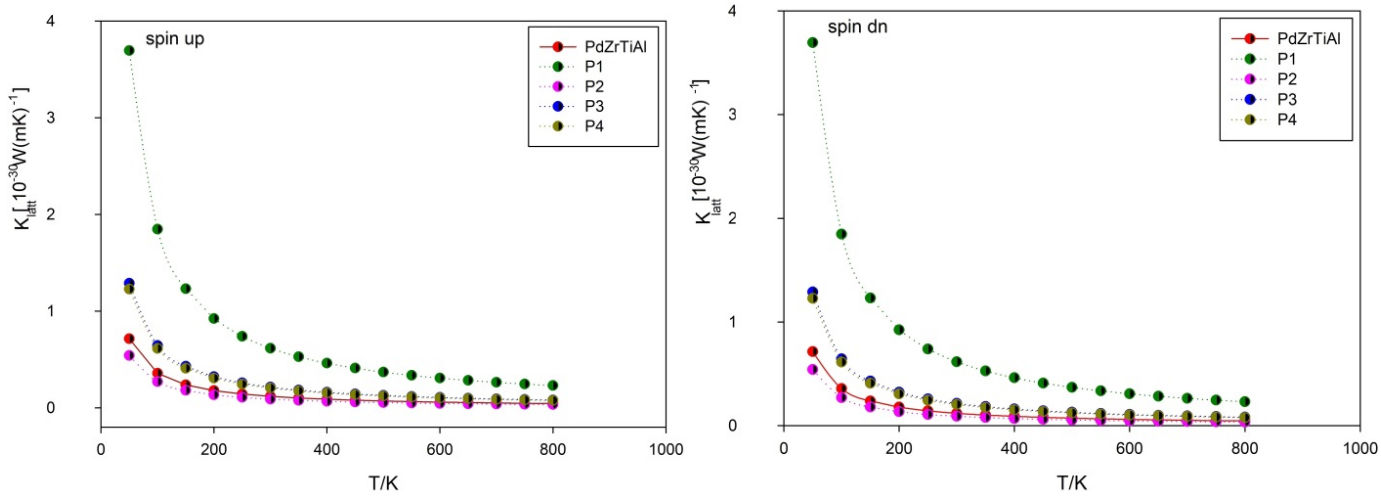

(f)

Fig. 4. The S, σ/τ, K_e/τ, PF, K_{latt} and ZT parameters of the PdZrTiAl versus temperature.

structure experiencing mechanical instability under strain and the stiffness properties increase totally in the applied pressure range. The calculation of the B/G and Poisson ratios showed that the PdZrTiAl has a ductile nature, and it has a low compression ratio versus the deformation, except for –8.1 GPa. Study of the transport properties of this composition reveals that the pressure has a slight effect on the electron contribution of the thermal conductivity in both spin directions, and the Seebeck coefficient escalate under stress. In the minority spin, the figure of merit has a value of about 1 in the room temperature range. Accordingly, the PdZrTiAl can be introduced as a suitable thermoelectric material to use in low temperature range.

Acknowledgment

This work is the result of the research project in the Kermanshah Branch, Islamic Azad University, Kermanshah, Iran.

REFRENCES

[1] G.Z. Xu, X.M. Zhang, Z.P. Hou, Y. Wang, E.K. Liu, X.K. Xi, S.G. Wang, W.Q. Wang, H.Z. Luo, W.H. Wang, G.H. Wu, EPL-Europhysics Lett. **111**, 68003 (2015).

[2] R.A. de Groot, F.M. Mueller, P.G. van Engen, K.H.J. Buschow, Phys. Rev. Lett. **50**, 2024 (1983).

[3] G.Y. Gao, K.-L. Yao, Appl. Phys. Lett. **103**, 232409 (2013).

[4] G. Gao, G. Ding, J. Li, K. Yao, M. Wu, M. Qian, Nanoscale **8**, 8986-8994 (2016).

[5] Y. Han, M. Wu, Y. Feng, Z. Cheng, T. Lin, T. Yang, R. Khenata, X. Wang, IUCrJ. **6**, 465-472 (2019).

[6] M.A. Carpenter, C.J. Howard, Acta Cryst. B **74**, 560-573 (2018).

[7] Y. Han, Z. Chen, M. Kuang, Zh. Liu, X. Wang, X. Wang, Results in Physics **12**, 435-446 (2019).

[8] Z. Li, Y. Jiang, Z. Li, C.F. Sánchez Valdés, J.L. Sánchez Llamazares, B. Yang, Y. Zhang, C. Esling, X. Zhao, L. Zuo, IUCrJ **5**, 54-66 (2018).

[9] J.-W. G. Bos, IUCrJ **4**, 712-713 (2017).

[10] Z. H. Liu, Z.J. Tang, J.G. Tan, Y.J. Zhang, Z.G. Wu, X.T. Wang, G.D. Liu, X.Q. Ma, IUCrJ **5**, 794-800 (2018) .

[11] A. Erkisi, G.Surucu, J. Polytechnic. **21** (4), 927-936 (2018).

[12] T. Li, R. Khenata, Zh. Cheng, H. Chen, H. Yuan, T. Yang, M. Kuang, S. B. Omrand , X. Wang, Acta Cryst. B **74**, 673-680 (2018).

[13] J.G. Tan, Z.H. Liu, Y.J. Zhang, G.T. Li, H.G. Zhang, G.D. Liu, X.Q. Ma, Results in Physics **12**, 1182-1189 (2019).

[14] S.V. Faleev, Y. Ferrante, J. Jeong, M.G. Samant, B. Jones, S.S.P. Parkin, Phyis. Rev. Appl. **7**, 034022 (2017).

[15] G. Qin, W. Wu, S. Hu, Y. Tao, X. Yan, Ch. Jing, X. Li, H. Gu, Sh. Cao, W. Ren, IUCrJ **4**, 506-511 (2017).

[16] Y. Han, M. Wu, M. Kuang, T. Yang, X. Chen, X. Wang, Results in Physics **11**, 1134-1141 (2018).

[17] I. Galanakis, P.H. Dederichs, N. Papanikolaou, Phys. Rev. B **66**, 174429 (2002).

[18] H. Lashgari, M.R. Abolhassani, A. Boochani, E. Sartipi, R. Taghavi-Mendi, A. Ghaderi, Indian J. Phys. **90**, 909 (2016).

[19] A. Anjami, A. Boochani, S.M. Elahi, H. Akbari, Results in Physics **7**, 3522 (2017).

[20] A. Planes, L. Mañosa, M. Acet, J. Phys. Condens. Matter. **21**, 233201 (2009).

[21] D. Do, M.S. Lee, S.D. Mahanti, Phys. Rev. B **84**, 125104 (2011).

[22] J. Winterlik, G.H. Fecher, A. Thomas, C. Felser, Phys. Rev. B **79**, 064508 (2009).

[23] T. Saito, N. Tezuka, M. Matsuura, S. Sugimoto, Appl. Phys. Exp. **6**, 103006 (2013).

[24] T. Kubota et al., Phys. Lett. **94**, 122504 (2009).

[25] S. Kasai et al., J. Appl. Phys. **115**, 173912 (2014).

[26] J. Winterlik et al., Adv. Mater. **24**, 6283 (2012).

[27] S. Ouardi, G.H. Fecher, C. Felser, J. Kübler, Phys. Rev. Lett. **110**, 100401 (2013).

[28] A. Kundu, S. Ghosh, R. Banerjee, S. Ghosh, B. Sanyal, Sci. Rep. **7**, 1803 (2017).

[29] V. Alijani et al., Phys. Rev. B **84**, 224416 (2011).

[30] L. Bainsla et al., J. Appl. Phys. **116**, 203902 (2014).

[31] V. Alijani, J. Winterlik, G.H. Fecher, S.S. Naghavi, C. Felser, Phys. Rev. B **83**,184428 (2011).

[32] G. Y. Gao, L. Hu, K.L. Yao, B. Luo, N. Liu, J. Alloy. Compd. **551**, 539-543 (2013).

[33] M. Singh, H.S. Saini, J. Thakur, A.H. Reshak, M.K. Kashyap, J. Alloy. Compd. **580**, 201-204 (2013).

[34] Y. Chen, Sh. Chen, B. Wang, B. Wu, H. Huang, X. Qin, D. Li, W. Yan, Appl. Sci. **9**, 620 (2019).

[35] L. Xiong, L. Yi, G.Y. Gao, J. Magn. Magn. Mater. **360**, 98-103 (2014).

[36] J.M.K. Al-Zyadi, G.Y. Gao, K.L. Yao, J. Magn. Magn. Mater. **378**, 1-6 (2015).

[37] G.Z. Xu et al., EPL-Europhysics Lett. **102**, 17007 (2013).

[38] K. Özdoğan, E. Şaşıoğlu, I. Galanakis, J. Appl. Phys. **113**, 193903 (2013).

[39] L. Bainsla, K.G. Suresh, Appl. Phys. Rev. **3**, 031101 (2016).

[40] Q. Gao, H.H. Xie, L. Li, G. Lei, J. Deng, X. Hu, Superlattice Microst. **85**, 536 (2015).

[41] X.T. Wang, T.T. Lin, H. Rozale, G.D. Liu, J. Magn. Magn. Mater. **402**, 190 (2016).

[42] A. Birsanc, Curr. Appl. Phys. **14**, 1434 (2014).

[43] P.-L. Yan, J.-M. Zhang, B. Zhou, Ke.-W. Xu, J. Phys. D **49**, 255002 (2016).

[44] H.-H. Xie, Q. Gao, L. Li, G. Lei, Ge-Y. Mao, X.-Ru. Hu, J.-B. Deng, Comput. Mater. Sci. **103**, 52-55 (2015).

[45] X. Wang, Z. Cheng, J. Wang, X. Wang, G. Liu, J. Mater. Chem. C **4**, 7176 (2016).

[46] X. Wang, Z. Cheng, J. Wang, G. Liu, J. Mater. Chem. C **4**, 8535 (2016).

[47] S. Berri, Chinese J. of Phys. **55**, 195-202 (2016).

[48] L.E. Bell, Science **321**, 1457-1461 (2008).

[49] Y. Cai, Y. Wang, D. Liu, Fu-Y. Zhao, Appl. Therm. Eng. **138**, 238-255 (2019).

[50] G.D. Mahan, Solid State Phys. **51**, 81 (1998).

[51] T. Plirdpring, K. Kurosaki, A. Kosuga, T. Day, S. Firdosy, V. Ravi, G.J. Snyder, Adv. Mater. **24**, 3622 (2012).
[52] M.L. Liu, I.W. Chen, F.Q. Huang, L.D. Chen, Adv. Mater. **21**, 3808-3812 (2009).
[53] F.J. Fan, B. Yu, Y.X. Wang, Y.L. Zhu, X.J. Liu, J. Am. Chem. Soc. **133**, 15910-15913(2011).
[54] R. Liu, L. Xi, H. Liu, X. Shi, W. Zhang, L. Chen, Chem. Commun. **48**, 3818-3820 (2012).
[55] A. Kosuga, K. Umekage, M. Matsuzawa, Y. Sakamoto, I. Yamada, Inorg. Chem. **53**, 6844-6849 (2014).
[56] J. Zhang, R. Liu, N. Cheng, Y. Zhang, J. Yang, C. Uher, X. Shi, L. Chen, W. Zhang, Adv. Mater. **26**, 3848-3853 (2014).
[57] V. Kucek, C. Drasar, J. Navratil, T. Plechacek, L. Benes, J. Phys. Chem. Solids. **83**, 18-23(2015).
[58] E.J. Skoug, J.D. Cain, D.T. Morelli, Appl. Phys. Lett. **98**, 261911 (2011).
[59] A. Suzumura, M.Watanabe, N. Nagasako, R. Asahi, Mater. **43**, 2356-2361 (2014).
[60] F.J. Fan, Y.X. Wang, X.J. Liu, L. Wu, S.H. Yu, Adv. Mater. **24**, 6158-6163 (2012).
[61] G. Zhong, K. Tse, Y. Zhang, X. Li, L. Huang, C. Yang, J. Zhu, Z. Zeng, Zh. Zhang, X. Xiao, Thin Solid Films **603**, 224 (2016).
[62] C. Sevik, T. Çağın, Appl. Phys. Lett. **95**, 112105 (2009).
[63] Ş. Ţălu, M. Bramowicz, S. Kulesza, A. Ghaderi, V. Dalouji, S. Solaymani, Z. Khalaj, Electron. Mater. Lett. **12**, 580-588 (2016).
[64] Ş. Ţălu, M. Bramowicz, S. Kulesza, A. Shafiekhani, M. Rahmati, A. Ghaderi, M. Ahmadirad, S. Solaymani, Surf. Interface Anal. **49** (3), 153-160 (2017).
[65] S. Solaymani, A. Ghaderi, L. Dejam, Ż. Garczyk, W. Sapota, S. Stach, V. Dalouji, C. Luna, S.M. Elahi, S.H. Elahi, Int. J. Hydrog. Eng. **42** (20), 14205-14219 (2017).
[66] T. Plirdpring, K. Kurosaki, A. Kosuga, T. Day, S. Firdosy, V. Ravi et al., Adv. Mater. **24**, 3622-3626 (2012).
[67] H. Liu, X. Shi, F. Xu, L. Zhang, W. Zhang, L. Chen et al., Nat. Mater. **11**, 422-425 (2012).
[68] W. Kohn, L.J. Sham, Phys. Rev. **140**, A1133 (1965).
[69] P. Blaha, K. Schwarz, P. Herzig, Phys. Rev. Lett. **54**, 1192 (1985).
[70] Ph. Haas, F. Tran, P. Blaha, K. Schwarz, R. Laskowsk, Phys. Rev. **B 80**, 195109 (2009).
[71] H.J. Monkhorst, J.D. Pack, Phys. Rev. B **13**, 5188 (1976).
[72] J.D. Pack, H.J. Monkhorst, Phys. Rev. B **16**,1748-1749 (1977).
[73] F. Murnaghan, Proc. Natl. Acad. Sci. USA. **30**, 244 (1944).
[74] W.C. Hu, Y. Liu, D.J. Li, X. Q. Zeng, C.S. Xu, Physica B. **427**, 85-90(2013).
[75] G.K.H. Madsen, D.J. Singh, Comput. Phys. Commun. **175**, 67 (2006).
[76] N.F. Mott, H. Jones, The Theory of the Properties of Metals and Alloys, Dover Publications, New York (1958).
[77] R. Hill, Proc. Phys. Soc. A **65**, 349 (1952).
[78] S.F. Pugh, Magn. **45**, 823-843 (1954).
[79] C. Jenkins, S.K. Khanna, New Insight into the Toughening Mechanisms of Seashell: From Arch Shape to Multilayer Structure, Academic Press, Cambridge, UK (2005).
[80] R. Iqbal, M. Bilal, S. Jalali Asadabadi, H.A.R. Aliabad, I. Ahmad, Int. J. Mod. Phys. B. **32**, 1850004 (2018).
[81] D.G. Pettifor, Mater. Sci. Technol. **8**, 345 (1992).
[82] P.H. Mott, J.R. Dorgan, C.M. Roland, J. Sound Vib. **312**, 572 (2008).
[83] Y. Tian, B. Xu, Z. Zhao, Int. J. Refract. Met. Hard Mater. **33**, 93-106(2012).
[84] D. Guo, Ch. Hu, Y. Xi, K. Zhang, J. Phys. Chem. C. **117**, 21597-21602 (2013).
[85] M. Irfan, Z. Abbas, S.A. Khan, M. Sohail, M. Rani, S. Azam, I.V. Kityk, J. Alloy. Comd. **750**, 804-810 (2018).
[86] A. Shafique, Y.-H. Shin, Sci. Rep. **7**, 1-10 (2017).
[87] F. Li, Z,Y. Wu, Z. Xu, X. Zhao, T. Zhu, J. Materiomics **4**, 208-214 (2018).
[88] G. Slack, J. Phys. Chem. Solids **34**, 321 (1973).